Jaesool Shim[1]
Prashanta Dutta[1]
Cornelius F. Ivory[2]

[1]School of Mechanical and Materials Engineering, Washington State University, Pullman, WA, USA
[2]School of Chemical Engineering and Bioengineering, Washington State University, Pullman, WA, USA

Received September 12, 2007
Revised November 27, 2007
Accepted November 28, 2007

Research Article

Effects of ampholyte concentration on protein behavior in on-chip isoelectric focusing

The effects of mobility corrections on carrier ampholytes are studied at various ampholyte concentrations to understand protein behavior during IEF. IEF simulations are conducted in the presence of 25 biprotic carrier ampholytes within a pH range of 6–9 after applying the Onsager–Debye–Hückel correction to the carrier ampholytes. Two model proteins with ten charge states but without ionic strength corrections are allowed to focus under an electric field of 300 V/cm in a 1 cm long channel. The IEF simulation results show that higher ionic strengths (50 – 100 mM) cause significant changes in the transient movement as well as the final focused profiles of both ampholytes and proteins. The time required for a single, well-defined peak to form increases with ionic strength when Onsager corrections are applied to the carrier ampholytes. For a particular ampholyte concentration, the space-averaged conductivity does not change during the final focusing stage, but the magnitude of space averaged conductivity is different for different ampholyte concentration. The simulation results also reveal that at steady-state ionic strength profiles remain flat throughout the channel except at the locations of proteins where a significant change in ampholyte concentration is obtained.

Keywords:
Ionic strength / Isoelectric focusing / Microchip / Onsager correction / Protein
DOI 10.1002/elps.200700683

1 Introduction

IEF is a powerful technique for separating charged particles or molecules such as DNA and proteins in response to an electric field. Since the 1980s, significant advances in carrier ampholyte-based IEF simulation have revolutionized the understanding of the electrophoretic process of charged molecules. Recent attention has been given to develop on-chip electrophoretic devices for drug discovery and clinical diagnostics due to their high resolution, fast separation, and cost effectiveness. The computer simulation of multi-dimensional IEF has grown rapidly in an effort to optimize chip design [1, 2].

In 1981, Palusinski *et al.* [3] introduced a computer model of IEF which could be used in a multicomponent system. Their mathematical model described how to predict the concentration of ampholytes, pH gradient, and conductance at the steady state. Later, Bier *et al.* [4] extended the model to apply to transient systems involving biprotic ampholytes (ampholytes with three charge states; -1, 0, $+1$). This unified model was able to predict the behavior of the four classical electrophoretic modes such as moving boundary electrophoresis (MBE), zone electrophoresis (ZE), ITP, and IEF. However, this model assumed constant absolute mobilities of carrier ampholytes as well as proteins in order to simplify the mathematical models and the numerical calculations.

Mosher *et al.* [5, 6] reported the IEF simulation with a more sophisticated model where protein mobility was corrected using the Debye–Hückel–Henry theory [7]. The main objective of that work was to predict the transient behavior of proteins more accurately during the IEF process by replacing the fixed, absolute mobility of proteins with a more accurate value of the mobility which is a strong function of ionic strength. Li *et al.* [8] studied the effect of ionic strength on the mobility of electrolyte buffer in CZE. In their work, they also discussed various models for electrophoretic mobility and activity coefficients. Dufreche *et al.* [9] presented the electrophoretic effect on the Onsager coefficients using a mean spherical approximation method for the equilibrium pair correlation function, which takes into account short-range interactions. Recently, Damme and Deconinck [10] derived an expression for the relaxation effect on the Onsager coeffi-

Correspondence: Professor Prashanta Dutta, School of Mechanical and Materials Engineering, Washington State University, Pullman, WA 99164-2920, USA
E-mail: dutta@mail.wsu.edu
Fax: +1-509-335-4662

Abbreviation: ZE, zone electrophoresis

cients for mixed electrolyte system based on the mean spherical approximation. Stoyanov *et al.* [11] obtained a simplified model to calculate the conductivity in the system using a lumped concentration of ampholytes instead of individual ampholyte concentrations and the results from that model showed a reasonable agreement with experimental data. In a series of publications [12–16], Gaš and co-workers presented a number of theoretical models to obtain corrected mobilities from limiting (absolute) mobilities of BGEs during CZE. In 2006, Hruška *et al.* [17] developed dynamic-based simulation software (Simul version 5), which can handle a variety of multivalent constituents with Onsager corrections for CZE and ITP. At the same time, Kantak *et al.* [18] showed the effect of carrier ionic strength in microscale cyclical electrical field-flow fractionation. In their work, they developed a lumped electrical parameter model for the corrected mobility of the carrier solution; their model predicts very well for carrier ionic strengths up to ~0.5 mM. In all previous work, the effects of ionic strength on carrier or BGEs were studied in ZE, capillary ZE, ITP, and cyclical electrical field-flow electrophoresis, but this phenomenon has not been investigated in IEF. Although the governing mathematical equations for ITP and IEF are identical, the time evolution and eventual "steady states" of ITP and IEF are very different. The acid–base behavior of the zwitterionic IEF ampholytes is distinct different from the buffering behavior of the ITP leading and terminating electrolytes (there is no counterion in IEF), and the role of the pH in these two techniques is also very different.

Recently, we developed a generalized 2-D (spatial) IEF model to study geometric effects on the transient focusing behavior of ampholytes and proteins using contraction–expansion microgeometries [2]. However, constant absolute mobility of ampholytes is assumed during IEF process in the 2-D (spatial) IEF model. In the present paper, we (i) include corrections to the ionic mobility of ampholytes using Onsager–Debye–Hückel theory, (ii) simulate the transient behavior of ampholytes and proteins at various ionic strengths based on limiting and corrected mobility, and finally (iii) discuss electrochemical phenomena such as pH profiles, space-averaged conductivity, and ionic strength profiles at steady state. To the best of our knowledge no previous study has demonstrated the effect of ionic strength on corrected mobility of carrier ampholyte in IEF. In this work, we are interested in studying the behavior of ampholytes and proteins at the transient processes as well as at the steady state to understand the effect of mobility correction.

2 Mathematical model of IEF

In this section, we present a generalized IEF model by removing the constraint that all ampholytes maintain constant absolute mobilities. In partially ionized solutes, the mobility of BGEs changes with ionic strength. Thus, to be more precise, ionic strength-dependent effective mobility of ampholytes should be considered in the IEF model.

In IEF, the concentration of *i*th component (C_i) is obtained by summing all *j* species (S_{ij}) in the system with a total of J_i dissociable groups, *i.e.*

$$C_i = \sum_{j=1}^{J_i+1} S_{ij} \tag{1}$$

The *i* components take into account all weak acids and bases, ampholytes, proteins, and even hydronium ions and hydroxyl ions. The effective mobility ($\langle \mu_i \rangle$) of a component, C_i, can be defined as follows,

$$\langle \mu_i \rangle = \frac{\sum_{j=1}^{J_i+1} \mu_{ij} S_{ij}}{C_i} \tag{2}$$

where μ_{ij} is the electrophoretic mobility of the *j* species that make up each *i* component in the system, respectively.

The mass conservation equation for each component (C_i) is obtained from the conservation equations of $J_i + 1$ species to yield

$$\frac{\partial C_i}{\partial t} - \nabla \cdot (D_i \nabla C_i) + \nabla \cdot \left[\vec{\mathbf{E}} \sum_{j=1}^{J_i+1} (\mu_{ij} S_{ij}) \right] = 0 \tag{3}$$

where $\vec{\mathbf{E}}$ is the electric field and D_i is the diffusion coefficient of component *i*. Then by combining Eqs. (2) and (3), we obtain

$$\frac{\partial C_i}{\partial t} + \nabla \cdot \left[\langle \mu_i \rangle \vec{\mathbf{E}} C_i - D_i \nabla C_i \right] = 0 \tag{4}$$

Equation (4) provides a single partial differential equation for each component. If the dissociation reactions are fast enough to be in equilibrium, J_i algebraic relations among the component *i* species can be obtained as

$$K_{ij} = \frac{C_H S_{ij}}{S_{ij+1}} \tag{5}$$

where C_H is the concentration of hydronium ions. For $j \geq 2$, the concentration of component and associated species are related by

$$C_i = S_{ij} \left(\prod_{k=1}^{j-1} \frac{K_{ik}}{C_H} \right) \left(1 + \sum_{jj=1}^{J_i} \prod_{k=1}^{jj} \frac{C_H}{K_{ik}} \right) \tag{6}$$

Now define the current density, $\vec{\mathbf{I}}$, and the charge density, ρ, as

$$\vec{\mathbf{I}} = F \sum_{i=1}^{M} \left(-D_i \nabla \left(\sum_{j=1}^{J_i+1} z_{ij} S_{ij} \right) + \vec{\mathbf{E}} \sum_{j=1}^{J_i+1} z_{ij} \mu_{ij} S_{ij} \right) \tag{7}$$

$$\rho = F\sum_{i=1}^{M}\left(\sum_{j=1}^{J_i+1} z_{ij}S_{ij}\right) = F\sum_{i=1}^{M}\langle z_i\rangle C_i \tag{8}$$

where z_{ij} is the valence, $\langle z_i\rangle$ the effective valence, F is the Faraday constant, and M is the number of components which include H_3O^+ and OH^- ions as $M-1$th and Mth components. For microfluidic applications where the charge density, $\rho \approx 0$, we obtain the electroneutrality constraint as

$$\rho = F\sum_{i=1}^{M}\langle z_i\rangle C_i = 0 \tag{9}$$

2.1 Onsager–Debye–Hückel theory

The properties of the ions in aqueous solutions such as ionic mobility, diffusivity, and conductivity are important factors to determine electrophoretic behavior. The mobility is influenced by the two phenomena: the relaxation effect and the electrophoretic effect. The former is a result of the asymmetric counter ion cloud that forms behind a moving ion while the latter is due to drag caused by the counter ions moving in the opposite direction. For the dilute aqueous solutions (less than 100 mM of ionic strength), the effective mobility, $\langle\mu_i\rangle$, of biprotic carrier ampholytes ($j = 1^+, 0, 1^-$) can be expressed as [14, 16]

$$\langle\mu_i\rangle = \frac{\mu_{i1^+}s_{i1^+} + \mu_{i1^-}s_{i1^-}}{s_{i1^+} + s_{i0} + s_{i1^-}} =$$

$$= \frac{\mu_{i1^+}10^{pK_{i1}^{mix}-pH} + \mu_{i1^-}10^{pH-pK_{i2}^{mix}}}{1 + 10^{pK_{i1}^{mix}-pH} + 10^{pH-pK_{i2}^{mix}}} \tag{10}$$

where $pK_{i1}^{mix} = -\log_{10}K_{i1}^{mix}$, $pK_{i2}^{mix} = -\log_{10}K_{i2}^{mix}$ and K_{i1}^{mix} and K_{i2}^{mix} are the mixed equilibrium constant [12]. For biprotic carrier ampholytes ($j = 1^+, 0, 1^-$), the corrected mobility of species (μ_{ij}) is given by the Onsager–Debye–Hückel equation [15] as

$$\mu_{i1^+} = \mu_{i1^+}^0 - \left(\mu_{i1^+}^0 z_{i1^+}|z_{i1^-}|B_1\frac{q_i}{1+\sqrt{q_i}} + B_2 z_{i1^+}\right)\frac{\sqrt{I_s}}{1+1.5\sqrt{I_s}} \tag{11}$$

$$\mu_{i1^-} = \mu_{i1^-}^0 - \left(\mu_{i1^-}^0 z_{i1^+}|z_{i1^-}|B_1\frac{q_i}{1+\sqrt{q_i}} + B_2|z_{i1^-}|\right)\frac{\sqrt{I_s}}{1+1.5\sqrt{I_s}} \tag{12}$$

where μ_{ij}^0 is the limiting mobility – mobility at the infinite dilution. I_s is the ionic strength of the solution, estimated as $I_s = \frac{1}{2}\sum_{i=1}^{M}\sum_{j=1}^{J_i+1} z_{ij}^2 S_{ij}$, and B_1 and B_2 are constants. For aqueous solutions at 25°C, $B_1 = 0.7817\ (\text{mM})^{-1/2}$ and $B_2 = 3.138E\text{-}04\ \text{cm}^2\text{s}^{-1}\ (\text{mM})^{-1/2}$. The parameter q_i is defined as [16]

$$q_i = \frac{z_{i1^+}|z_{i1^-}|}{z_{i1^+} + |z_{i1^-}|}\left(\frac{\mu_{i1^+}^0 + \mu_{i1^-}^0}{|z_{i1^-}|\mu_{i1^+}^0 + z_{i1^+}\mu_{i1^-}^0}\right) \tag{13}$$

For a symmetrical electrolyte ($z_{i1^+} = -z_{i1^-} = z_{ij}$), $q_i = 1/2$. For biprotic ampholytes, the mixed equilibrium constants can be obtained from equilibrium constant as [14]

$$K_{i1}^{mix} = \frac{\gamma_{i1^+}K_{i1}}{\gamma_{i0}} \tag{14}$$

$$K_{i2}^{mix} = \frac{\gamma_{i0}K_{i2}}{\gamma_{i1^-}} \tag{15}$$

where γ_{ij} is the activity coefficient, and it is related to the ionic strength as

$$\gamma_{i0} = 1 \tag{16a}$$

$$\log\gamma_{i1^\pm} = \frac{-Az_{i1^\pm}^2\sqrt{I_s}}{1+1.5\sqrt{I_s}} + 0.1z_{i1^\pm}^2 I_s \tag{16b}$$

A is a constant, which for aqueous solution at 25°C acquires value of $A = 0.5085\ (\text{mM})^{-1/2}$. The above equations show that mixed equilibrium constants depend on the ionic strength of the solution. For example, at an ionic strength of $I_s = 8.2$ mM, the mixed equilibrium constants (pK_{i2}^{mix}) become 0.96 and 1.96 if the equilibrium constants of an ampholyte (pK_{i2}) are 1.0 and 2.0, respectively. It is important to note that the Onsager–Debye–Hückel model works for low molecular weight components such as ampholytes but that it cannot be applied to high molecular weight proteins. Hence, in this study, these corrections are not applied to model proteins.

3 Computational model and assumptions

The model is based on the mass conservation relations given by Eq. (4), an electroneutrality condition of the form

$$C_H - \frac{K_W}{C_H} = -\sum_{i=1}^{M-2}\langle z_i\rangle C_i \tag{17}$$

and the charge conservation equation ($\nabla\cdot\vec{\mathbf{I}} = 0$) as

$$\nabla\cdot\left[\sum_{i=1}^{M}\sum_{j=1}^{J_i+1} z_{ij}\mu_{ij}S_{ij}\vec{\mathbf{E}}\right] = \sum_{i=1}^{M}\sum_{j=1}^{J_i+1} z_{ij}D_{ij}\nabla^2 S_{ij} \tag{18}$$

The concentrations of amphoteric molecules are obtained from the component equations. The concentration of hydronium is calculated from the electroneutrality equation, while the hydroxyl concentration is obtained from the equilibrium relationship ($K_W = C_{OH}C_H$), where K_W is the equilibrium constant for water. The electric field $\left(\vec{\mathbf{E}} = -\nabla\phi\right)$ is calculated from the charge conservation equation shown in Eq. (18).

It is assumed that during IEF, all ionic components including water are in chemical equilibrium which implies that the ionic reactions are fast enough that the individual components remain in a pseudoequilibrium state. In this study, each ampholyte is considered as biprotic, *i.e.*, the two dissociation constants on either side of their p*I*'s dominate the transient behavior of the carrier ampholytes. For biprotic ampholytes, the Onsager–Debye–Hückel theory is applied to obtain the ionic strength dependence on the mobility of species (μ_{ij}) from the limiting mobility (μ_{ij}^0). In addition, the activity coefficients are calculated by the Mclnnes approximation to the Debye–Hückel formulation in order to acquire ionic strength-dependent equilibrium constant [16]. The ionic strength-dependent effective mobility, $\langle\mu_i\rangle$, of each ampholyte is computed using Eq. (10).

Figure 1 shows the dependence of the ionic strengths on the corrected mobilities of ampholyte species. Three different cases of limiting mobilities ($\mu_{i1^+}^0$) are considered to demonstrate the effect of ionic strength on the corrected mobilities of species. An identical corrected mobility distribution is also obtained for $\mu_{i1^-}^0$ (not shown here). It is clear that actual mobility decreases from the infinite dilute states as the buffer ionic strength increases due to the net effects of the Onsager corrections mentioned earlier, variations in the ionic activity coefficient with ionic strength and variations in the ampholyte dissociation constants with ionic strength. The decay rate is very fast at low ionic strength, but it becomes linear at higher ionic strengths (I_s>35 mM). In IEF, the ionic strength changes with time until a final focal point is reached. Hence, the mobility of ampholytes is affected significantly.

The diffusion coefficient of biprotic ampholytes is calculated as

$$D_i = D_{i1^\pm} = \frac{RT}{F}\left|\frac{\mu_{i1^\pm}}{z_{i1^\pm}}\right| = \frac{RT}{F}|\mu_{i1^\pm}| \tag{19}$$

Model proteins, each having ten charge states, are allowed to focus in the microchannel. The effective mobility of each protein is calculated as $\langle\mu_i\rangle = \omega_i\langle z_i\rangle$, where ω_i is the absolute mobility and $\langle z_i\rangle$ is the effective valence which is a function of equilibrium constants and hydronium concentration. The effective valence of proteins and ampholytes is calculated using the expression $\langle z_i\rangle C_i = \sum_{j=1}^{J_i+1} z_{ij} S_{ij}$. Note that in the dissociation reaction equations (Eq. 5), mixed equilibrium constants are used for ampholytes while equilibrium constants are employed for proteins.

In this study, the absolute mobility of each species is kept constant ($\omega_{ij} = \omega_i$) for a particular protein and ionic strength corrections are not applied to the protein mobilities. Moreover, for proteins, the Nernst–Einstein equation ($D_i = RT\omega_i/F$) is used to calculate the diffusion coefficient from the absolute mobility, where R is the gas constant and T is the absolute temperature.

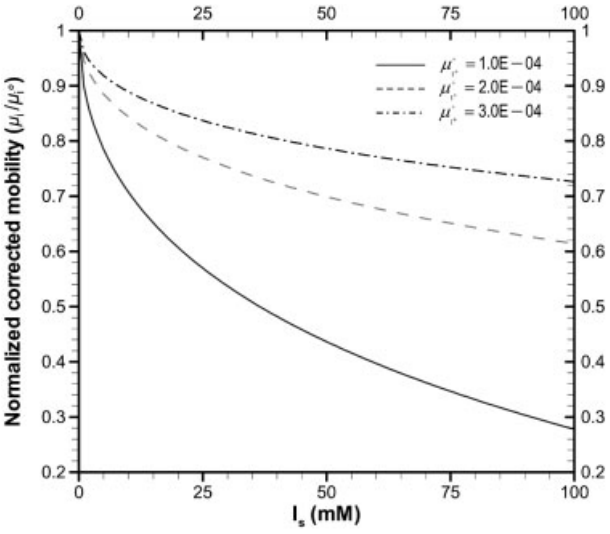

Figure 1. Effects of ionic strengths on the corrected mobility of ampholyte species. All parameters are based on aqueous solutions at 25°C. At very low ionic strength the corrected mobility approaches the limiting mobility.

This model neglects Joule heating since relatively smaller electric fields are used for separation. Electric field-induced electrokinetic flow is not considered here because in IEF experiments, the channel is generally coated with methylcellulose or other chemicals to suppress electroosmosis [19, 20].

4 Results and discussion

The effects of ionic strength on the mobility of biprotic ampholytes during IEF are obtained numerically. A 2D finite volume method is developed to solve the mass conservation equations with electromigration and diffusion given by Eq. (4) together with the charge conservation equation defined in Eq. (18). Details of the numerical scheme and boundary conditions are presented in our earlier publication [2]. Two model proteins with isoelectric points (p*I*'s) 7.48 and 8.38 are allowed to focus in the presence of 25 carrier ampholytes within a pH range of 6 to 9 ($\Delta pI = 0.125$) under a nominal electric field of 300 V/cm. Proteins are modeled as having ten charge states, while ampholytes are based on three charge states (j = 1^+, 0, 1^-). Consideration of polyvalent proteins is especially important to understand the focusing behavior of proteins with time. The physicochemical properties of proteins are presented in Table 1. Initially both proteins and ampholytes are uniformly distributed throughout the channel. Three different ampholyte concentration cases are studied here, and, in all cases, the initial concentration of ampholytes is 10 times of that of proteins. The numerical results are obtained for a 2-D straight (planar) channel as shown in Fig. 2, and all results are extracted at the channel

Table 1. Electrochemical properties of model proteins used in the IEF simulation

p*K*	Model protein 1 (p*I* = 7.48)	Model protein 2 (p*I* = 8.38)
pK_1	6.3	5.5
pK_2	6.5	6.1
pK_3	7.12	6.8
pK_4	7.25	7.15
pK_5	7.5	7.22
pK_6	8.5	8.19
pK_7	9.8	8.58
pK_8	10.31	9.5
pK_9	11.18	9.55

The initial (uniform) concentrations of each protein for low, medium, and high cases are 0.01, 0.1, and 1.0 mM, respectively. The absolute mobilities for proteins 1 and 2 are 3.79*E*-05 and 3.16*E*-05 $cm^2/V \cdot s$, respectively.

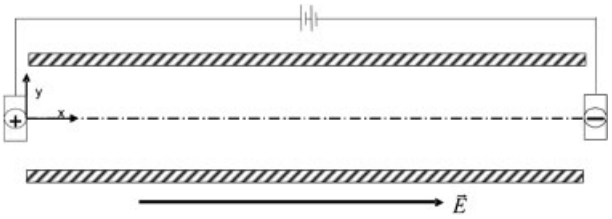

Figure 2. Scheme of a 2-D planar channel (1 cm × 100 μm) used to simulate ampholyte-based IEF in a pH range of 6–9. The anodic potential is 300 V at the left, while the cathode is set to be ground (0 V) at the right. The limiting mobilities of each ampholyte are $-2.02E{-}04$ and $2.02E{-}04$ cm^2/Vs for negative and positive charge states, respectively. The ΔpK ($pK_2 - pK_1$) for each ampholyte is 2.5.

centerline. However, this numerical model can be used to simulate any 2-D microgeometries such as T-junction, cross-channel, dog-leg channels, *etc.*

4.1 Effects on transient focusing behavior

The effects of the ionic mobility correction (Onsager correction) of ampholytes on the transient behavior of ampholytes and proteins are shown in Fig. 3. For comparison purposes, the transient electrophoretic behavior of amphoteric molecules is also presented by maintaining a constant absolute mobility (without Onsager correction) of the ampholytes. That means, for the no correction case, the ionic strength is set to zero in Eqs. (10)–(16). Three different initial (uniform) ampholyte concentrations (low: 0.1 mM, medium: 1 mM, and high: 10 mM) are considered corresponding to the initial ionic strengths of 0.53, 5.37, and 56.1 mM. It is important to note that the Onsager–Debye–Hückel theory can only be applied for ionic strengths less than 100 mM. Hence, the initial concentration of ampholytes is set such that the ionic strength remains below 100 mM. Although 25 biprotic ampholytes are used in the numerical simulation, only five selected ampholytes (p*I*'s = 6.875, 7.675, 8.0, 8.375, and 8.75) are presented for clarity. During the transient period, all ampholytes and proteins initially form pairs of peaks on the anodic and cathodic edges of the channel (Figs. 3a, c, and e), which move toward the channel center and form one peak (Figs. 3b, d, and f) for each component.

Figures 3a and b show the transient electrophoretic behavior of proteins and ampholytes at low ampholyte concentration (initial ionic strength = 0.53 mM, initial ampholyte concentration = 0.1 mM) at 20 and 100 s, respectively. Numerical results reveal that at low ampholyte concentration (ionic strength), the ampholytes with Onsager correction slightly lag behind those without Onsager correction at the initial stage of the focusing (Fig. 3a), while the proteins move at the same speed regardless of the Onsager correction. The slower speed of ampholyte peak formation predicted by the Onsager correction is due to the reduction in the absolute mobility with ionic strength as shown in Fig. 1. However, at the final stages of focusing (at 100 s), the ampholytes and proteins are shaped in a similar fashion and are being focused with very little difference (Fig. 3b) for both cases. In other words, at low ampholyte concentration, the influence of ionic strength on ampholyte mobility is negligible in the final focusing stages. This is due to the fact that in the final stages of IEF the ionic strength goes down significantly from the initial value, and the actual mobility of ampholytes approaches the limiting mobility throughout the channel. For instance, the final ionic strength becomes 0.13 mM (except at the location of protein) if the initial ionic strength is 0.53 mM.

The behavior of proteins and ampholytes at medium ampholyte concentration (initial ionic strength = 5.37 mM, initial ampholyte concentration = 1 mM) is shown in Figs. 3c and d for the initial and final stages of focusing, respectively. Similar to the previous case, the ampholytes with the Onsager correction move more slowly than those without the Onsager correction. In addition, protein peaks travel at different rates to their p*I*s with and without the Onsager correction. However, in the final stages of focusing, the deviation in concentration profiles of ampholytes and proteins reduces between with and without Onsager correction cases as the buffer achieves low ionic strength during the final focusing stages. From Figs. 3a–d, it is clear that at any stage in the focusing process, the concentration distribution of proteins and ampholytes depends on the initial ionic strength of the system.

Similar trends are also observed for high ampholyte concentration (initial ionic strength = 56.1 mM, initial ampholyte concentration = 10 mM). Figures 3e and f show the concentration profiles of proteins and ampholytes for high initial ionic strength. In this case, the mobility of ampholyte with Onsager correction is much less than without the Onsager correction at both initial (20 s) and final (100 s) focusing stages. Hence, the shape of the concentra-

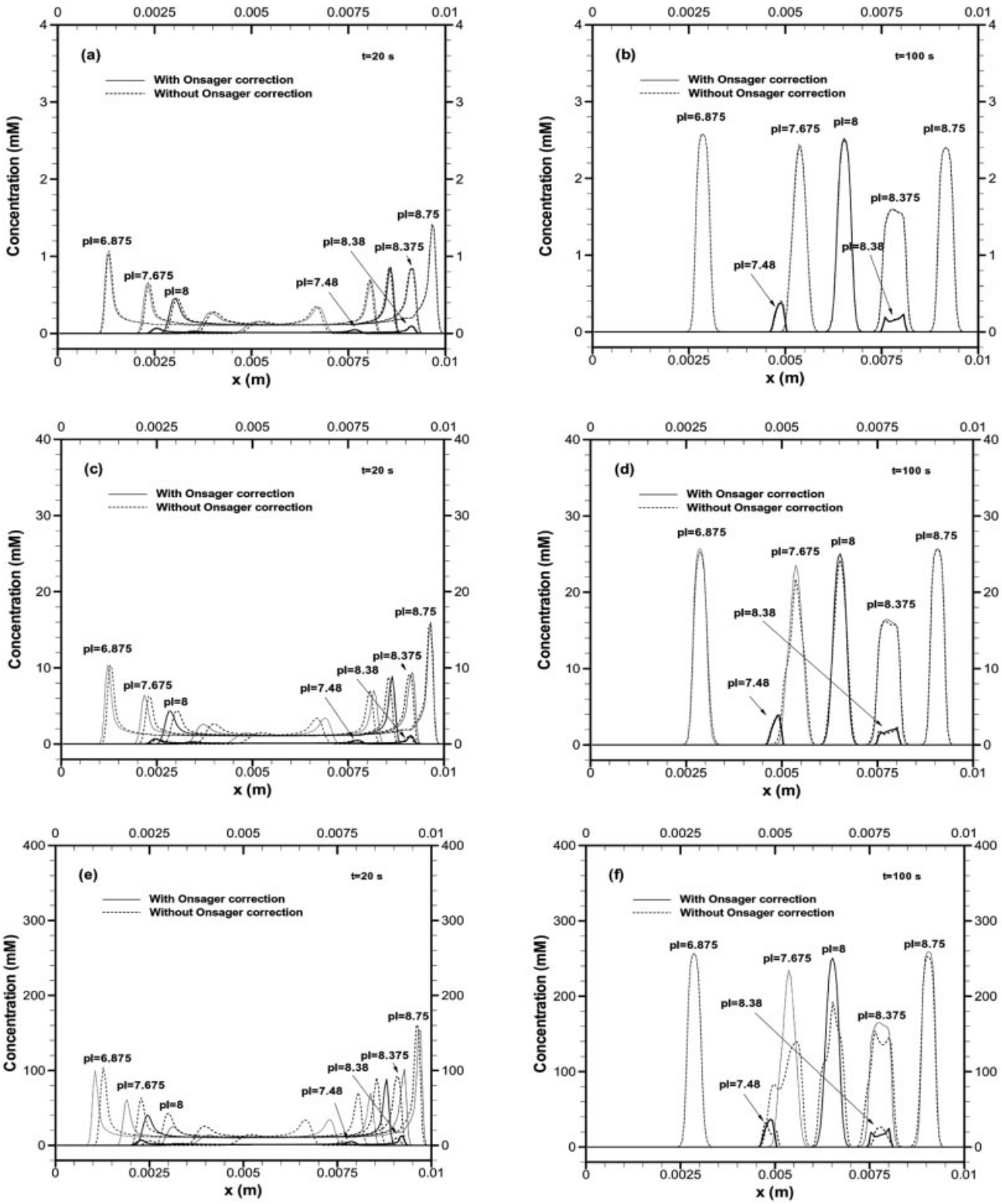

Figure 3. Comparison of transient behaviors of ampholytes and proteins with and without Onsager correction for (a, b) low ampholyte concentration (initial ionic strength: I_s = 0.53 mM and initial concentration of ampholyte: C_o = 0.1 mM), (c, d) medium ampholyte concentration (initial ionic strength: I_s = 5.37 mM and initial concentration of ampholyte: C_o = 1.0 mM), and (e, f) high ampholyte concentration (initial ionic strength: I_s = 56.1 mM and initial concentration of ampholyte: C_o = 10 mM. Figures (a), (c), and (e) are obtained in an early stage of focusing (20 s), while (b), (d), and (f) are acquired in a final stage of focusing (100 s). The nominal electric field used for this simulation is 300 V/cm.

tion profiles deviates noticeably between with and without the Onsager correction due to the different speed of focusing.

4.2 Effect on the focused ampholytes and proteins

Figure 4 shows the steady state behavior of all ampholytes and proteins for different ampholyte concentrations. The simulation data revealed that all 25 carrier ampholytes and model proteins are completely focused and stationary at 170 s under a constant voltage of 300 V in the 1 cm long channel. One interesting observation is that the ampholytes near the p*I*s of two proteins are focused with slightly different shapes. Specifically, the focused peaks of the ampholytes (# 12, 13, and 20) are lower than the other ampholytes and the shapes of these ampholytes are not symmetric. If there were no proteins, all ampholytes should have formed a Gaussian profile with uniform peak height. This discrepancy in concentration profiles of ampholytes 12, 13, and 20 are due to the presence of proteins at their locations. In our simulation, the p*I* of model protein 1 is only 0.02 pH unit away from the p*I* of ampholyte #13 (p*I* = 7.50) and the p*I* of model protein 2 is 0.005 pH unit away from the p*I* of ampholyte 20 (p*I* = 8.375). In other words, protein 2 is sitting almost on top of ampholyte 20, while protein 1 is in between ampholyte 12 and 13. These results reveal that the closer the p*I* values of a protein and its neighboring ampholyte are, the less symmetric and non-Gaussian will be the profiles of protein and ampholyte. The shapes of the two focused proteins are different due to the different mobility and diffusion coefficients.

To understand the effect of the corrected mobility on the steady state focusing behavior, the concentration profiles of focused ampholytes and proteins with the Onsager correction are also compared to those without the Onsager correction in Fig. 4. For low initial ionic strengths (Fig. 4a), the concentration profiles of the focused proteins and ampholytes are very similar regardless of the Onsager correction. These results tell us Onsager correction is not required for on-chip IEF with low ampholyte concentrations. Figure 4b reveals that the focused shapes of ampholytes and proteins with and without Onsager correction when the initial ionic strength is $I_s = 5.37$ mM. In this case, the concentration profiles of ampholytes are very similar for both with and without Onsager correction, but the protein profiles start deviating. However, when it comes to high initial ionic strength ($I_s = 56.1$ mM), the ampholyte positions with Onsager correction are slightly shifted from those without Onsager correction. These shifts in focused positions can be explained from the pH profile presented in Fig. 5. In Figs. 5a and b, the pH curves are not different between with and without Onsager correction at both low and mid initial ionic cases ($I_s < 5.37$ mM). But, in the case of high initial ionic strength ($I_s = 56.1$ mM), the pH curve is slightly shifted toward the electrodes. Therefore, the shifted positions of ampholyte with and without correction are caused by the fact

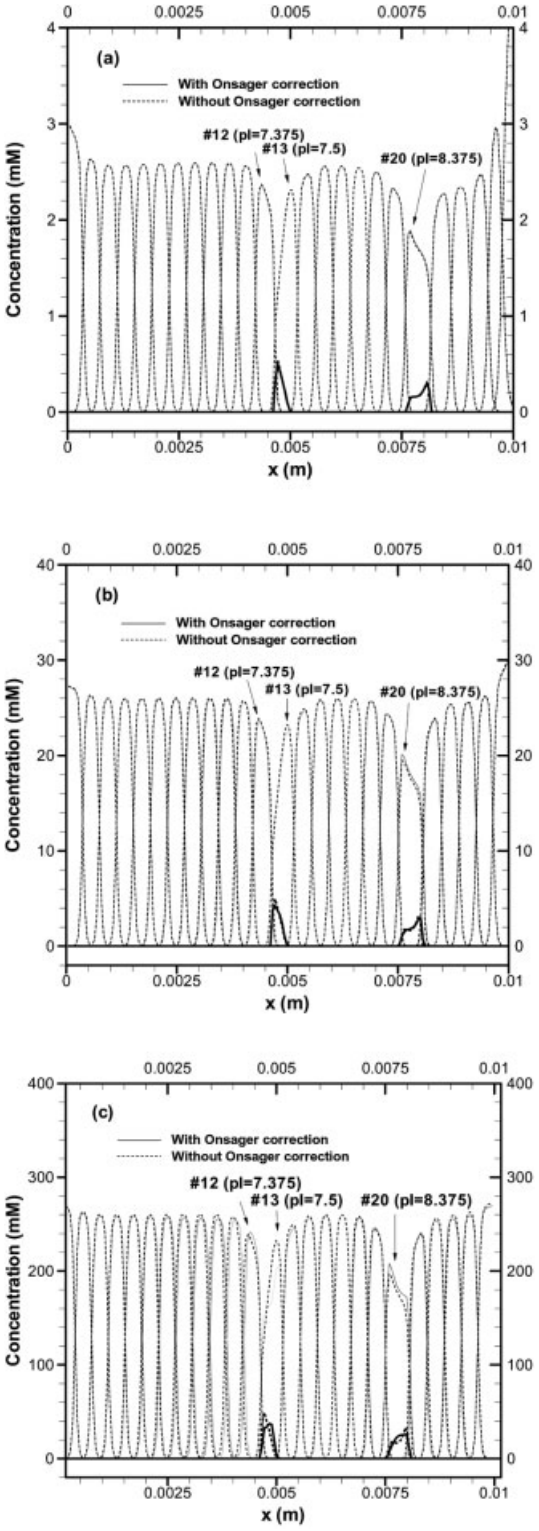

Figure 4. Comparison of steady-state behaviors of ampholytes and proteins with and without Onsager correction for (a) low ampholyte concentration, (b) medium ampholyte concentration, (c) high ampholyte concentration at 170 s. All other conditions remain the same as in Fig. 3. The time to reach the steady state varies from case to case.

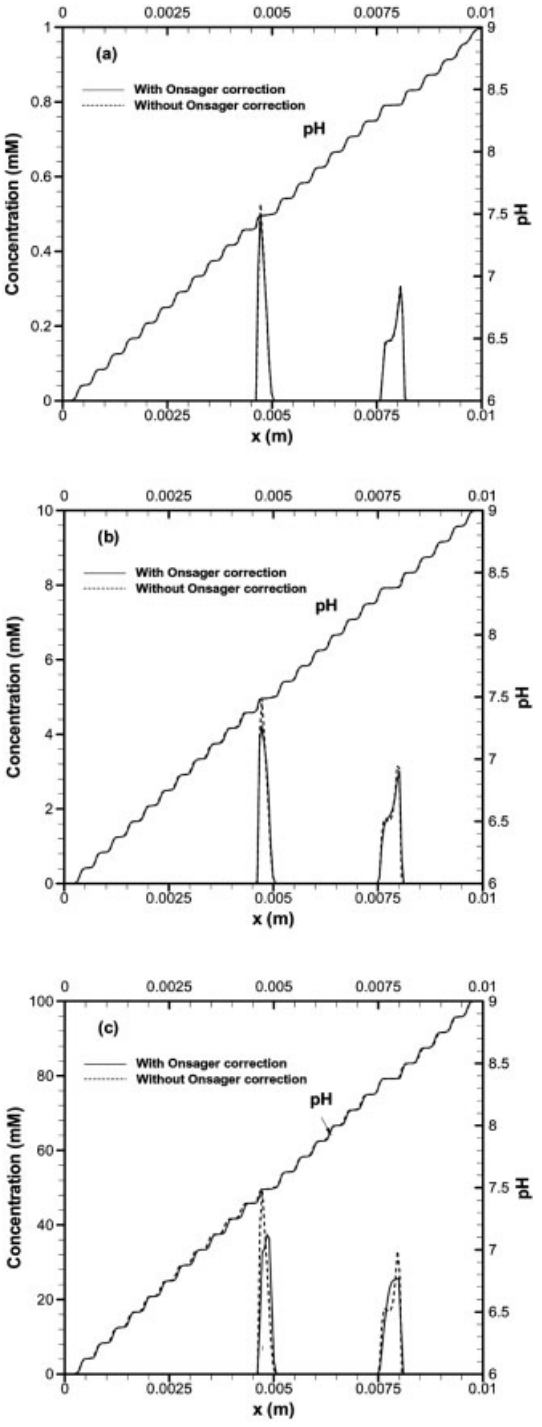

Figure 5. Effect of Onsager correction on pH curves and focused protein profiles at steady state for (a) low ampholyte concentration, (b) medium ampholyte concentration, and (c) high ampholyte concentration. All other conditions remain same as Fig. 4.

that the pH profile changes at high ampholyte concentration. It is important to note that the focused positions of two proteins are identical with and without correction because the pH curves are overlapped at focusing positions of proteins. Thus, it can be concluded that the focused positions of proteins are the same at steady state for with and without Onsager correction.

The focusing time and the merging time of proteins are also obtained. The focusing time is defined as the time required reaching steady state, while the merging time is defined as the required time for a double peak of a protein becomes a single peak [22]. In the case of low and mid initial ionic strength, the merging time and focusing times are observed the same with and without Onsager correction as 97 and 170 s. However, in the case of high initial ionic strength, the focusing times are almost the same with and without correction, but the merging times are different for with (109 s) and without Onsager correction (97 s).

4.3 Space-averaged conductivity and ionic strength

Conductivity of buffer electrolyte plays a crucial role in the transient IEF process. To achieve higher resolution and faster separations, higher electric fields are generally applied in microchip IEF. However, high electric field might produce excessive heat in the microsystem if the ionic conductivity of the system is also very high, especially in the early stages of focusing. For this reason, low conductivity of carrier ampholytes is preferred to avoid severe Joule heating in the microchip. To determine the effects of ampholyte concentration on the conductivity distribution we define a space-averaged conductivity as $\bar{\sigma} = \frac{1}{LW}\int_0^L \int_0^W \left(F \sum_{i=1}^{M} \sum_{j=1}^{J_i+1} z_{ij}\mu_{ij}S_{ij}\right) \mathrm{d}y\mathrm{d}x$, where L and W are the length and width of the channel, respectively.

Figure 6 shows the transient space-averaged conductivity profiles for different ampholyte concentrations. Our simulations show that the space-averaged conductivity drops expo-

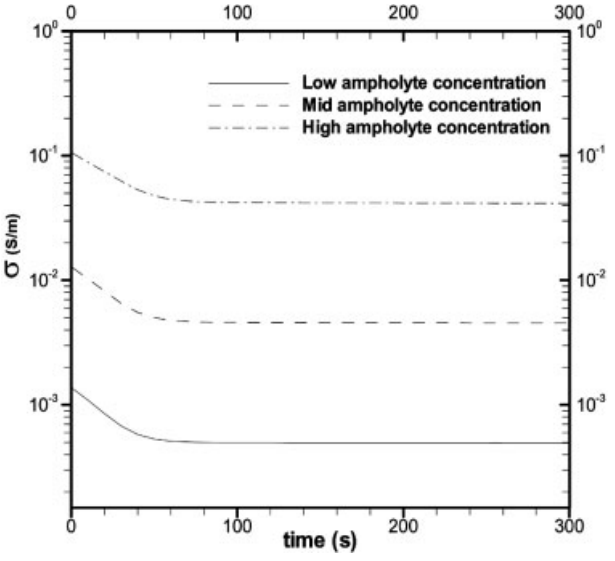

Figure 6. Transient space-averaged conductivity profiles at various ampholyte concentrations.

nentially in the initial stages of focusing, but it stabilizes in the final stages of focusing. This is a hallmark of ampholyte-based transient IEF process. In addition, the conductivity change is connected to the formation of pH gradient. Figure 6 also implies that the current in the system drops sharply in the initial stages of focusing when constant potentials are used in electrode reservoirs. Although the final focused states of the proteins are obtained at 170 s from the initiation of the electric field, the conductivity profile is presented until 300 s to demonstrate the steady behavior in the system. The simulated trends of conductivity are in a good agreement with literature [10].

The steady state ionic strength distribution is presented in Fig. 7 for all three cases shown earlier. In the final stage, ionic strengths are uniformly distributed except near two proteins where two peaks are observed. These peaks are due to the multiple (10) charge states of model proteins, although the concentration of protein is small compare to carrier ampholytes. The distinct shapes of these two peaks are related to the concentration profiles of the proteins at those locations (see Figs. 4 and 5). Our numerical results show that the final ionic strength depends on the initial concentration of ampholytes.

5 Concluding remarks

The effects of ionic strength on ampholyte and protein behavior are investigated in carrier ampholyte-based IEF. To obtain the corrected mobility of ampholyte species, the Onsager–Debye–Hückel theory is employed as a function of ionic strength and the McInnes approximation is applied for the activity coefficient. Twenty-five biprotic carrier ampholytes are used for a pH range of 6–9 in a 1 cm channel length and two model proteins with ten charge states are focused under 300 V. Three initial ionic strengths (0.53, 5.37, and 56.1 mM) are considered for the IEF simulations to study the transient and final focused behavior of both ampholytes and proteins. Numerical results show that the higher ionic strength changes the effective mobility of biprotic ampholytes, and the shapes of ampholytes and proteins are different in transient states. However, the effect of Onsager correction is minimal at low ionic strengths where the mobilities of the ampholytes approach their limiting value. For any ampholyte concentration, the space-averaged conductivity profile decreases abruptly at the initial stages of focusing, but it flattens at the final stages of separation. At the final stage of focusing the ionic strength remains flat, except in the neighborhood of the two model proteins. Our numerical results show that the merging time varies with initial ionic concentrations, while the focusing time remains almost the same for all ionic strengths. Although a 2-D (spatial) numerical model is used in this study, the results obtained from the straight microchannel vary only in the longitudinal direction. Hence, these results could be applied to any 1-D geometry such as capillary tube or straight microchannel.

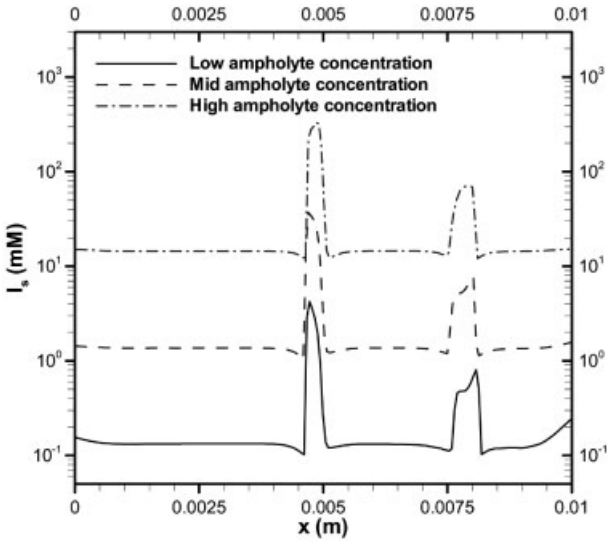

Figure 7. Ionic strength distribution along the microchannel for various concentrations of ampholytes at 170 s.

This work was supported by the National Science Foundation under grant no. CBET0626471.

The authors have declared no conflict of interest.

6 References

[1] Chatterjee, A., *J. Micromech. Microeng.* 2003, *13*, 758–767.

[2] Shim, J., Dutta, P., Ivory, C. F., *Electrophoresis* 2007, *28*, 572–586.

[3] Palusinski, O. A., Allgyer, T. T., Mosher, R. A., Bier, M., *Biophys. Chem.* 1981, *13*, 193–202.

[4] Bier, M., Palusinski, O. A., Mosher, R. A., Saville, D. A., *Science* 1983, *219*, 2181–2187.

[5] Mosher, R. A., Dewey, D., Thormann, W., Saville, D. A., Bier, M., *Anal. Chem.* 1989, *61*, 362–366.

[6] Mosher, R. A., Gebauer, P., Caslavska, J.,Thormann, W., *Anal. Chem.* 1992, *64*, 2991–2997.

[7] Henry, D. C., *Proc. R. Soc. Lond. Ser. A* 1931, *133*, 106–129.

[8] Li, D., Fu, S., Lucy, C. A., *Anal. Chem.* 1999, *71*, 687–699.

[9] Dufreche, J. F., Bernard, O., Turq, P., *J. Chem. Phys.* 2002, *116*, 2085–2097.

[10] Damme, S. V., Deconinck, J., *J. Phys. Chem. B* 2007, *111*, 5308–5315.

[11] Stoyanov, A. V., Das, C., Fredrickson, C. K., Fan, Z. H., *Electrophoresis* 2005, *26*, 473–479.

[12] Jaros, M., Vcelakova, K., Zusková, I., Gaš, B., *Electrophoresis* 2002, *23*, 2667–2677.

[13] Muzikar, J., Goor, T. V. D., Gaš, B., Kenndler, E., *Electrophoresis* 2002, *23*, 375–382.

[14] Vcelakova, K., Zuskova, I., Kenndler, E., Gaš, B., *Electrophoresis* 2004, *25*, 309–317.

[15] Koval, D., Kašička, V., Zusková, I., *Electrophoresis* 2005, *26*, 3221–3231.

[16] Zusková, I., Novotna, A., Vcelakova, K., Gaš, B., *J. Chromatogr. B* 2006, *841*, 129–134.

[17] Hruška, V., Jaros, M., Gaš, B., *Electrophoresis* 2006, *27*, 984–991.

[18] Kantak, A. S., Srinivas, M., Gale, B. K., *Anal. Chem.* 2006, *78*, 2557–2564.

[19] Cui, H., Horiuchi, K., Dutta, P., Ivory, C. F., *Anal. Chem.* 2005, *77*, 1303–1309.

[20] Cui, H., Horiuchi, K., Dutta, P., Ivory, C. F., *Anal. Chem.* 2005, *77*, 7878–7886.

[21] Patankar, S. V., *Numerical Heat Transfer and Fluid Flow*, Hemisphere, New York 1980.

[22] Shim, J., Dutta, P., Ivory, C. F., *J. Nanosci. Nanotechnol.* 2007, in press.

